APLF (C2orf13) is a Novel Human Protein Involved in the Cellular Response to Chromosomal DNA Strand Breaks

Article (Published Version)

APLF (C2orf13) Is a Novel Human Protein Involved in the Cellular Response to Chromosomal DNA Strand Breaks

Natasha Iles, Stuart Rulten, Sherif F. El-Khamisy and Keith W. Caldecott

***Mol. Cell. Biol.* 2007, 27(10):3793. DOI: 10.1128/MCB.02269-06.**
Published Ahead of Print 12 March 2007.

MOLECULAR AND CELLULAR BIOLOGY, May 2007, p. 3793–3803 Vol. 27, No. 10
0270-7306/07/$08.00+0 doi:10.1128/MCB.02269-06

APLF (C2orf13) Is a Novel Human Protein Involved in the Cellular Response to Chromosomal DNA Strand Breaks[▽]

Natasha Iles,[1]† Stuart Rulten,[1]† Sherif F. El-Khamisy,[1,2] and Keith W. Caldecott[1]*

Genome Damage and Stability Centre, University of Sussex, Falmer, Brighton, Sussex BN25 3EU, United Kingdom,[1] and Biochemistry Department, Faculty of Pharmacy, Aim Shams University, P.O. Box 11566, Cairo, Egypt[2]

Received 5 December 2006/Returned for modification 4 January 2007/Accepted 5 March 2007

Aprataxin and polynucleotide kinase (PNK) are DNA end processing factors that are recruited into the DNA single- and double-strand break repair machinery through phosphorylation-specific interactions with XRCC1 and XRCC4, respectively. These interactions are mediated through a divergent class of forkhead-associated (FHA) domain that binds to peptide sequences in XRCC1 and XRCC4 that are phosphorylated by casein kinase 2 (CK2). Here, we identify the product of the uncharacterized open reading frame C2orf13 as a novel member of this FHA domain family of proteins and we denote this protein APLF (*a*prataxin- and *P*NK-*l*ike *f*actor). We show that APLF interacts with XRCC1 in vivo and in vitro in a manner that is stimulated by CK2. Yeast two-hybrid analyses suggest that APLF also interacts with the double-strand break repair proteins XRCC4 and XRCC5 (Ku86). We also show that endogenous and yellow fluorescent protein-tagged APLF accumulates at sites of H_2O_2 or UVA laser-induced chromosomal DNA damage and that this is achieved through at least two mechanisms: one that requires the FHA domain-mediated interaction with XRCC1 and a second that is independent of XRCC1 but requires a novel type of zinc finger motif located at the C terminus of APLF. Finally, we demonstrate that APLF is phosphorylated in a DNA damage- and ATM-dependent manner and that the depletion of APLF from noncycling human SH-SY5Y neuroblastoma cells reduces rates of chromosomal DNA strand break repair following ionizing radiation. These data identify APLF as a novel component of the cellular response to DNA strand breaks in human cells.

DNA single- and double-strand breaks are induced through a variety of ways, including the direct attack of deoxyribose by reactive oxygen species. DNA strand breaks can pose a considerable threat if not rapidly repaired or responded to appropriately, as indicated by the increased genetic instability, cancer frequency, or neurodegenerative pathology observed in diseases in which such processes are absent or attenuated. While the overall mechanisms by which DNA single- and double-strand breaks are repaired are very different, the repair of all such strand breaks requires a number of common enzymatic steps (7). For example, most DNA breaks arising endogenously in cells require end processing activities to restore damaged DNA termini to 3′ hydroxyl and 5′ phosphate configurations, and in the final repair step, all DNA breaks require a DNA ligase to reestablish the integrity of the phosphodiester backbone.

DNA end processing is perhaps the most enzymatically diverse step of DNA strand break repair, primarily because of the broad range of termini that can arise. One enzyme implicated in the repair of oxidative DNA termini at both DNA single- and double-strand breaks is polynucleotide kinase (PNK) (10, 33). PNK associates with the DNA single-strand break repair (SSBR) and double-strand break repair (DSBR) protein complexes through direct interaction with casein kinase 2 (CK2)-phosphorylated XRCC1 and XRCC4, respectively (16, 21). These interactions are mediated through a divergent forkhead-associated (FHA) domain in PNK that can specifically target CK2-phosphorylated peptides. Intriguingly, the protein aprataxin, which is mutated in the neurodegenerative disease ataxia-oculomotor apraxia type 1, possesses a similar FHA domain and binds the same CK2-phosphorylated regions of XRCC1 and XRCC4 (6, 11, 12–14, 22, 25). Aprataxin is also an end processing enzyme, repairing abortive 5′ AMP intermediates of DNA ligase activity (1). In the current study, we identify a third member of the aprataxin- and PNK-like FHA domain family which we denote APLF (*a*prataxin- and *P*NK-*l*ike *f*actor). We demonstrate that APLF is a novel component of the cellular response to chromosomal DNA single- and double-strand breaks.

MATERIALS AND METHODS

DNA constructs and recombinant proteins. To create pGBKT7-APLF, the human APLF open reading frame (ORF) was amplified from the C2orf13 IMAGE clone 6042653 (MRC GeneService) by PCR using the primers 5′-AAAA CCATGGCAATGTCCGGGGGCTTCGAGCTG-3′ (the NcoI site and the APLF start codon are underlined) and 5′-TTGAATTCGGCAGATATGACTA CAGAA-3′ (the EcoRI site and the stop codon are underlined) and subcloned into the NcoI/EcoRI sites of pGBKT7 (Clontech). To create pcD2E-His-Myc-APLF, the APLF ORF was amplified from IMAGE clone 6042653 by PCR using the primers 5′-AAA*GAATTC*CCGCC*ATG*CATCACCATCACCATCACCCG*G AGGAGCAGAAGCTGATCTCAGAGGAGGACCTG*TCCGGGGGCTTCGA GCTGCAG-3′ (the EcoRI site and the APLF start codon are underlined, and the His_6 and Myc tags are italicized) and 5′-AAAGAATTCGGATTCCTATTT TCTTTTCATAAACC-3′ (the EcoRI site and the stop codon are underlined) and subcloned into the EcoRI sites of the mammalian expression vector pcD2E (15). To create pET16b-APLF, a fragment encoding APLF was removed from pGBKT7-APLF and subcloned into pET16b (Novagen) by using NdeI and BamHI. To create pET16b-APLF$^{1-166}$, pET16b-APLF was linearized with AvrII and the 5′ overhangs filled in with Klenow polymerase prior to religation. pET16b-APLF$^{1-166}$ encodes a polypeptide of 168 amino acids, of which 166

* Corresponding author. Mailing address: Genome Damage and Stability Centre, University of Sussex, Falmer, Brighton, Sussex BN1 9RQ, United Kingdom. Phone: 44 (0) 1273 877519. Fax: 44 (0) 1273 678121. E-mail: k.w.caldecott@sussex.ac.uk.

† These authors contributed equally to this work.

▽ Published ahead of print on 12 March 2007.

encode the amino-terminal region of APLF. To create pET16b-APLF$^{360-511}$, pET16b-APLF was cut with SphI and the resulting 3′ overhang filled in with Klenow fragment. A 0.5-kb fragment encoding the C-terminal region of APLF was then released with BamHI and subcloned into the blunted NdeI/BamHI sites of pET16b. To create pEYFP-C1-APLF, the APLF ORF was amplified from IMAGE clone 6042653 by PCR using the primers 5′-AAAGAATTCCATGTC CGGGGGCTTCGAGCTG-3′ (the EcoRI site and the APLF start codon are underlined) and 5′-AAAGAATTCGGATTCCTATTTTCTTTTCATAAAC C-3′ (the EcoRI site and the stop codon are underlined) and subcloned into the EcoRI sites of pEYFP-C1 (Clontech). To create pEYFP-C1-APLF^{R27A}, pEYFP-C1-APLF^{zfm1}, and pEYFP-C1-APLF^{zfm2}, the APLF ORF in pEYFP-C1-APLF was mutated by site-directed mutagenesis using a QuikChange mutagenesis kit and the appropriate primers (Stratagene). To create pEYFP-nls-APLF, pEYFP-nls-APLF^{R27A}, and pEYFP-nls-APLF^{zfm1}, the simian virus 40 (SV40) large T-antigen nuclear localization signal was engineered into the relevant fusion protein between the APLF sequence and its N-terminal yellow fluorescent protein (YFP) tag by subcloning the annealed oligonucleotides 5′-T CGAGCCCCTAAGAAAAAGCGGAAGGTGCA-3′ and 5′-AGCTTGCACC TTCCGCTTTTTCTTAGGGGC-3′ into the XhoI/HindIII sites within the multiple cloning site of the appropriate pEYFP-C1-APLF construct.

To create pRFP-C1-XRCC1, the XRCC1 ORF was amplified from pcD2EXH (8) by PCR using the primers 5′-AAGAATTCTATGCCGGAGATCCGCCTC CGCC-3′ (the EcoRI site and the XRCC1 start codon are underlined) and 5′-TTGTCGACTCAGGCTTGCGGCACCACCCCATAGAG-3′ (the SalI site and the stop codon are underlined) and subcloned into the EcoRI/SalI sites of pRFP-C1 encoding monomeric red fluorescent protein (mRFP) (9). To create pRFP-C1-XRCC4, the XRCC4 ORF was subcloned from pCI-neo-Myc-XRCC4 (kindly provided by Queti Riballo and Elaine Taylor) into pRFP-C1 by using EcoRI and XbaI. All recombinant histidine-tagged proteins expressed in *Escherichia coli* were expressed in BL21(DE3) and purified by metal chelate affinity chromatography using nickel-nitrilotriacetic acid agarose (QIAGEN).

Protein slot blots and far-Western blotting. Recombinant XRCC1-His (10 μg) expressed in and purified from bacteria (see above) was phosphorylated with CK2 in 90-μl reaction mixtures containing 10 mM $MgCl_2$, 1 mM ATP, 13.3 mM HEPES, pH 8, 80 mM NaCl, and 0.67 mM dithiothreitol (DTT) at 30°C for 30 min. Mock phosphorylation reactions lacked CK2 or XRCC1, as indicated. For slot blot experiments, mock phosphorylation reactions and aliquots of CK2 phosphorylation reactions (0.125 to 1 μg of XRCC1-His as indicated) were slot blotted under a vacuum, in quadruplicate, onto Hybond-C nitrocellulose membranes. The membranes were air dried and one strip stained with amido black. The remainder were blocked in binding buffer (20 mM HEPES, 50 mM NaCl, 1 mM DTT) containing 2% (wt/vol) nonfat dried milk (NFDM) at room temperature for 4 h. Blots were then washed (three times for 5 min each) with binding buffer lacking NFDM and incubated with 5 μg of full-length recombinant His-APLF, His-APLF$^{1-166}$, or His-APLF$^{360-511}$ in binding buffer at 4°C overnight. Blots were then washed (three times for 5 min each) in binding buffer and incubated in binding buffer containing 2% NFDM and affinity-purified anti-APLF polyclonal antibody (SK3595) at a dilution of 1 in 500 at room temperature for 4 h. The blots were then washed (three times for 10 min each) in binding buffer and incubated in binding buffer containing 2% NFDM and goat anti-rabbit horseradish peroxidase-conjugated secondary antibody at a dilution of 1 in 5,000 at room temperature for 1 h. Finally, following further washes in binding buffer (three 5-min washes), antibody complexes were detected by enhanced chemiluminescence (ECL Plus; Amersham Biosciences) and autoradiography. SK3595 was raised by Eurogentec and affinity purified against recombinant human APLF expressed and purified from *E. coli*.

For far-Western blotting, 3 μg of full-length recombinant His-APLF, His-APLF$^{1-166}$, or His-APLF$^{360-511}$ was fractionated in quadruplicate by sodium dodecyl sulfate (SDS)-polyacrylamide gel electrophoresis (PAGE) and transferred to a Hybond-C nitrocellulose membrane. The membrane was stained with Ponceau S to confirm equal loading and transfer and then destained. Proteins were denatured and renatured by sequential incubations (10 min each) with decreasing concentrations (6 M to 0.19 M) of guanidine-HCl essentially as described previously (23). Membranes were then incubated at 4°C overnight with 2 ml 1% NFDM-HYB100 containing recombinant XRCC1-His (10 μg) prephosphorylated in 90-μl reaction mixtures (at 30°C for 30 min) containing 10 mM $MgCl_2$, 1 mM ATP, 13.3 mM HEPES, pH 8, 80 mM NaCl, 0.67 mM DTT, and rat liver CK2 (kindly provided by Flavio Meggio and Lorenzo Pinna). Mock phosphorylation reactions lacked CK2 or XRCC1-His, as indicated. Filters were then washed with 1% NFDM-HYB100 and the membranes incubated with anti-XRCC1 polyclonal antibody (SK3188) at a dilution of 1 in 1,000 in 1% NFDM-HYB100 at room temperature for 2 h. The membranes were then washed (three times for 10 min each) with 1% NFDM-HYB100 and incubated with goat anti-rabbit horseradish peroxidase-conjugated secondary antibody at a dilution of 1 in 5,000 in 1% NFDM-HYB100 at room temperature for 30 min. Following further washes (three 10-min washes) with 1% NFDM-HYB100, antibody complexes were detected by enhanced chemiluminescence (ECL Plus; Amersham Biosciences) and autoradiography.

Anti-APLF (SK3595) and anti-XRCC1 (SK3188) polyclonal antibodies were raised by Eurogentec against recombinant human APLF and XRCC1 from *E. coli* and insect cells, respectively, and were affinity purified against the appropriate recombinant proteins from *E. coli*.

Yeast two-hybrid analyses. *Saccharomyces cerevisiae* Y190 cells were transformed with the indicated pACT and PGBKT7 constructs and transformants selected on minimal medium plates (glucose plus yeast nitrogen base without amino acids) additionally containing adenine and histidine. Pooled populations of transformants were streaked onto two minimal medium plates with adenine and histidine and one minimal medium plate with adenine and 50 mM 3-amino-1,2,4-triazole. The activation of the *His3* reporter gene was indicated by comparative growth on minimal medium plates containing adenine and 3-amino-1,2,4-triazole and minimal medium plates containing adenine and histidine after 4 to 6 days at 30°C. The activation of the β-galactosidase (β-Gal) reporter gene was determined by qualitative X-Gal (5-bromo-4-chloro-3-indolyl-β-D-galactopyranoside) assays on colony filter lifts from minimal medium plates containing adenine and histidine. Quantitative β-Gal assays were conducted essentially as described by Clontech (Yeast Protocols Handbook). Equivalent expression levels of DNA binding domain or activation domain fusion proteins were confirmed by Western blotting both for cell cultures employed for filter lift β-Gal assays and for quantitative β-Gal assays. Cell extracts were prepared in cracking buffer (8 M urea, 5% [wt/vol] SDS, 40 mM Tris-HCl [pH 6.8], 0.1 mM EDTA, 0.4 mg/ml bromophenol blue, 1% β-mercaptoethanol, 1× protease inhibitor cocktail [Sigma]) and fractionated by SDS-PAGE, and Myc-tagged APLF (expressed from pGBKT7) was detected by immunoblotting with anti-Myc monoclonal antibody (MAb) (9B11; Cell Signaling Technology) and DNA binding domain fusion proteins by immunoblotting with polyclonal anti-GAL4 activation domain antibody (Upstate Biotechnology). Washed membranes were then incubated with the appropriate horseradish peroxidase-conjugated secondary antibody (Dako) and bound antibodies visualized using enhanced chemiluminescence (Amersham Biosciences).

Immunoprecipitations. For immunoprecipitation experiments, ~3×10^7 HeLa cells were transiently transfected with pcD2E vector or pcD2E-His-Myc-APLF by using GeneJuice transfection reagent (Novagen) and pooled populations of transfected cells were selected in medium containing G418 (0.8 mg/ml) for 5 days. Alternatively, ~3×10^7 A549 cells were stably transfected with pCD2E and either empty pSUPER or pSUPER encoding the APLF RNA interference (RNAi) sequence GAAGAAATCTGCAAAGATA (pSUPER-APLF) by selection with 0.8 mg/ml G418 for 4 weeks. Transfected cells were lysed in 3 ml lysis buffer (20 mM Tris-HCl, pH 7.5, 10 mM EDTA, 100 mM NaCl, 1% Triton X-100, 0.5 mM sodium orthovanadate, 50 mM sodium fluoride, 10 mM β-glycerophosphate, and 1× protease inhibitor cocktail [Sigma]) on ice for 5 min. Clarified extracts were diluted to 2 mg/ml in lysis buffer and 3 ml of each extract precleared for 1 h at 4°C with 60 μl protein G-Sepharose beads (Sigma). HeLa cell extract (1.5 ml) was incubated with 1 μl of either anti-Myc MAb (9B11) or anti-Flag MAb (M2; Sigma) and A549 cell extract (1.5 ml) with either 100 μl anti-XRCC1 polyclonal antibody (SK3188) or 0.01 μl rabbit immunoglobulin G (IgG; Dako) overnight at 4°C with gentle agitation. Each sample was then incubated with 30 μl protein G-Sepharose beads for 1 h at 4°C with gentle agitation. The beads were then washed three times with lysis buffer (300 μl each wash) and bound proteins eluted by heating with 55 μl of 2× SDS-PAGE sample buffer at 90°C for 5 min. Clarified protein samples were fractionated by SDS-PAGE, transferred to nitrocellulose, and immunoblotted with anti-Myc MAb (9B11) or either anti-XRCC1 (SK3188) or anti-APLF (SK3595) polyclonal antibody.

Direct and indirect immunofluorescence experiments. For direct immunofluorescence experiments, *XRCC1* mutant EM9 (30, 31) or *XRCC4* mutant XR-1 (20, 28) CHO cells seeded onto coverslips were transfected with the indicated enhanced YFP or mRFP fusion protein constructs by using GeneJuice transfection reagent (Novagen). After 24 h, cells were washed with phosphate-buffered saline (PBS) and mock treated or treated with 10 mM hydrogen peroxide in PBS for 10 min at room temperature, washed with PBS, and then incubated in drug-free media at 37°C for 20 to 120 min. The coverslips were then washed in PBS and fixed (5 min in 4% paraformaldehyde in PBS). Fixed cells were then permeabilized in 0.2% Triton X-100 for 2 min, washed with PBS, and stained with 0.000025% DAPI (4′,6′-diamidino-2-phenylindole) for 5 min. Coverslips were mounted in Vectashield (Vector Labs) and analyzed with a Zeiss Axioplan 2 fluorescence microscope. Photographs were taken at a magnification of ×100

and YFP-APLF-transfected cells scored for subcellular localization of YFP-APLF.

For indirect immunofluorescence experiments, A549 cells were seeded onto gridded coverslips (MatTek) in 10-cm dishes at ~1×10^4 cells/cm^2 and, after 2 days, preincubated for 10 min with 10 μg/ml Hoechst dye 33258 at 37°C. Selected cells were then irradiated with a 351-nm UVA laser focused through a 40×/1.2-W objective using a Zeiss Axiovert equipped with LSM 520 Meta. UVA (10.47 μJ) was introduced to an area of approximately 15 μm by 2 μm (approximately 0.35 μJ/μm^2). After exposure, coverslips were incubated at 37°C for the times indicated and washed in ice-cold PBS, and cells were fixed in ice-cold methanol-acetone (1:1) for 5 min and then permeabilized for 5 min in PBS-0.1% Tween. Coverslips were incubated in PBS-5% NFDM for 30 min for blocking and then overnight at 4°C in PBS-1% NFDM containing anti-XRCC1 MAb (clone 33-2-5) and anti-APLF polyclonal antibody (both at 1/200 dilutions). Coverslips were then incubated with secondary labeling with Alexa Fluor 555 anti-mouse and Alexa Fluor 488 anti-rabbit antibodies (1/200 in PBS-1% milk; Invitrogen) for 1 hour at room temperature. DNA was stained with 0.1 μg/ml DAPI (Sigma). Tracks were then visualized using a Nikon Eclipse 50i microscope fitted with a ×100 oil immersion objective.

Chromosomal DNA strand break repair assays. To knock down APLF in SH-SY5Y cells, 2×10^6 cells were cotransfected with pCD2E vector (2 μg) and either pMAX-GFP vector (4 μg; Amaxa), pSUPER vector harboring the APLF RNAi sequence GAAGAAATCTGCAAAGATA (4 μg), or 160 pg of the XRCC1 small interfering RNA (siRNA) duplex GCCUGAAGUAUGUGCUA UAdTdT (sense strand; QIAGEN) by using Nucleofector and Nucleofector kit V (Amaxa). Twenty-four hours after nucleofection, cells were placed into a mild selection/differentiation medium containing 0.25 mg/ml G418 and 10 μM all-*trans* retinoic acid to induce neuronal differentiation. After 3 days of selection, the medium was replaced with medium containing 10 μM retinoic acid only. For alkaline comet assays, 5×10^5 SH-SY5Y cells were harvested 6 days after transfection and irradiated (20 Gy of gamma rays) before being returned to 37°C for 7.5, 15, or 30 min. At each time point, 1×10^5 treated cells were removed and DNA damage was measured by single-cell agarose gel electrophoresis, essentially as described previously (5). For γ-H2AX assays, A549 cells stably transfected with pCD2E and either empty pSUPER or pSUPER encoding the APLF RNAi sequence GAAGAAATCTGCAAAGATA, or SH-SY5Y cells 6 days after transient transfection with green fluorescent protein, pSUPER-APLF, or XRCC1 siRNA as described above, were grown on glass coverslips and exposed to 1 to 3 Gy of γ-radiation before being returned to 37°C. At the times indicated, coverslips were washed in PBS, fixed (5 min in 4% paraformaldehyde in PBS), permeabilized (0.2% Triton X-100 for 2 min), blocked (5% NFDM for 30 min), and incubated with anti-γ-H2AX MAb (clone JBW301, 1/800 in 1% NFDM in PBS; Upstate). Cells were then washed (three times for 5 min each) in PBS containing 0.1% Tween 20 and 0.02% SDS and incubated for 1 h with Alexa Fluor 488 goat anti-mouse IgG secondary antibody (1/200 dilution in 1% milk-PBS). The cells were then washed (five times for 5 min each) as described above, mounted in Vectashield (Vector Labs), and scored for γ-H2AX foci by using a Nikon Eclipse 50i microscope.

DNA damage-induced modification of APLF. Subconfluent 1BR3, FD105 (AOA1), or AT7BI (A-T) primary fibroblasts were harvested, either exposed to gamma rays (3 Gy) or treated with 10 mM H_2O_2 on ice for 20 min, and then incubated at 37°C for 20 min (H_2O_2) or 30 min (gamma rays) in drug-free media. Cells were then harvested and lysed in SDS-PAGE sample buffer, and aliquots of cell extracts were fractionated by SDS-PAGE (7.5% gels) and immunoblotted with anti-APLF polyclonal antibody (SK3595).

RESULTS

Database analyses identified a third protein that contains an FHA domain with sequence similarity to the FHA domains present in PNK and aprataxin (Fig. 1A). In particular, the putative FHA domain in this protein, which is the 511-amino-acid product of the previously uncharacterized ORF C2orf13 (Swiss-Prot accession no. Q8IW19), contains a number of basic residues that are predicted to promote the interaction with peptides phosphorylated by CK2 (2, 34). We thus denoted this protein APLF. BLAST analyses with the human APLF protein sequence identified putative homologues in a broad range of organisms from flies to humans and revealed that APLF is comprised of two highly conserved regions separated by a poorly conserved central region (Fig. 1B). Whereas the conserved amino terminus encodes the FHA domain, the conserved C-terminal region includes two short motifs that are repeated in tandem and strongly resemble C_2H_2 zinc fingers (ZnFs). The C-terminal region also possesses a highly acidic C-terminal tail. BLAST analyses with the C-terminal region identified 18 additional proteins that contain the ZnF motif in a range of organisms, though only in APLF homologues was the motif present in duplicate (Fig. 1C). The ZnF is highly conserved both in primary sequence and in the spacing between the putative zinc coordinating residues and is configured $CX_5CX_6HX_5H$. Strikingly, many of the proteins containing the APLF-like ZnF are involved in DNA strand break repair and/or contain domains implicated in DNA metabolism, including four homologues of tyrosyl phosphodiesterase 1, three poly(ADP-ribose) polymerase 1-like proteins, and homologues of DNA ligase III and Ku70.

We first examined whether, like PNK and aprataxin, APLF interacts with the DNA strand break repair proteins XRCC1 and XRCC4. Indeed, APLF interacted with both of these proteins in yeast two-hybrid analyses but did not interact with several other DNA strand break repair proteins, including aprataxin and DNA ligase IIIα (Fig. 2A). We showed previously that neither XRCC1 nor XRCC4 transactivates the His3 or β-Gal reporter genes in these assays by itself (11). In addition, endogenous XRCC1 was immunoprecipitated from Myc-APLF-transfected HeLa cell extracts by anti-Myc antibodies but was not immunoprecipitated by control anti-FLAG antibodies (Fig. 2B, upper panel) or by anti-Myc antibodies from untransfected cells (Fig. 2B, lower panel). More importantly, immunoprecipitation of endogenous XRCC1 from the human A549 cell extract, which we detected using both standard anti-XRCC1 polyclonal antibodies and antibodies specific for CK2-phosphorylated XRCC1(pS485/pT488) (21, 22), corecovered endogenous APLF, confirming that APLF is a bona fide component of the single-strand break repair machinery (Fig. 2C, left panel). That it was APLF that was recovered and detected in these experiments was confirmed by its absence from A549 cells in which APLF was depleted (Fig. 2C, middle and right panels). Interestingly, we noted in these and other experiments (Fig. 3A) that APLF migrates much more slowly than expected during SDS-PAGE, at a position expected for a polypeptide of ~75 kDa, most likely due to the acidic C-terminal tail.

The interactions of aprataxin and PNK with XRCC1 and XRCC4 are greatly stimulated by the phosphorylation of the latter proteins with CK2 (11, 16, 21, 22). To examine whether this was true for APLF, we purified from *E. coli* full-length histidine-tagged human His-APLF, an amino-terminal fragment of His-APLF containing the FHA domain (His-APLF$^{1-166}$), and a C-terminal fragment of His-APLF (His-APLF$^{360-511}$) containing the putative C_2H_2 ZnFs (Fig. 3A). We then mock phosphorylated or CK2 phosphorylated recombinant human XRCC1-His in vitro and incubated the slot blotted products of these reactions with recombinant His-APLF protein probes. To confirm that XRCC1-His was successfully phosphorylated by CK2, we employed two phospho-specific anti-XRCC1 antibodies raised against the CK2 phosphorylation sites pS485/pT488 and pS518/pS519/pS523 (Fig. 3B) (22). Whereas both His-APLF and His-APLF$^{1-166}$ preferentially interacted with CK2-phosphorylated XRCC1-His (Fig. 3C, top left and middle

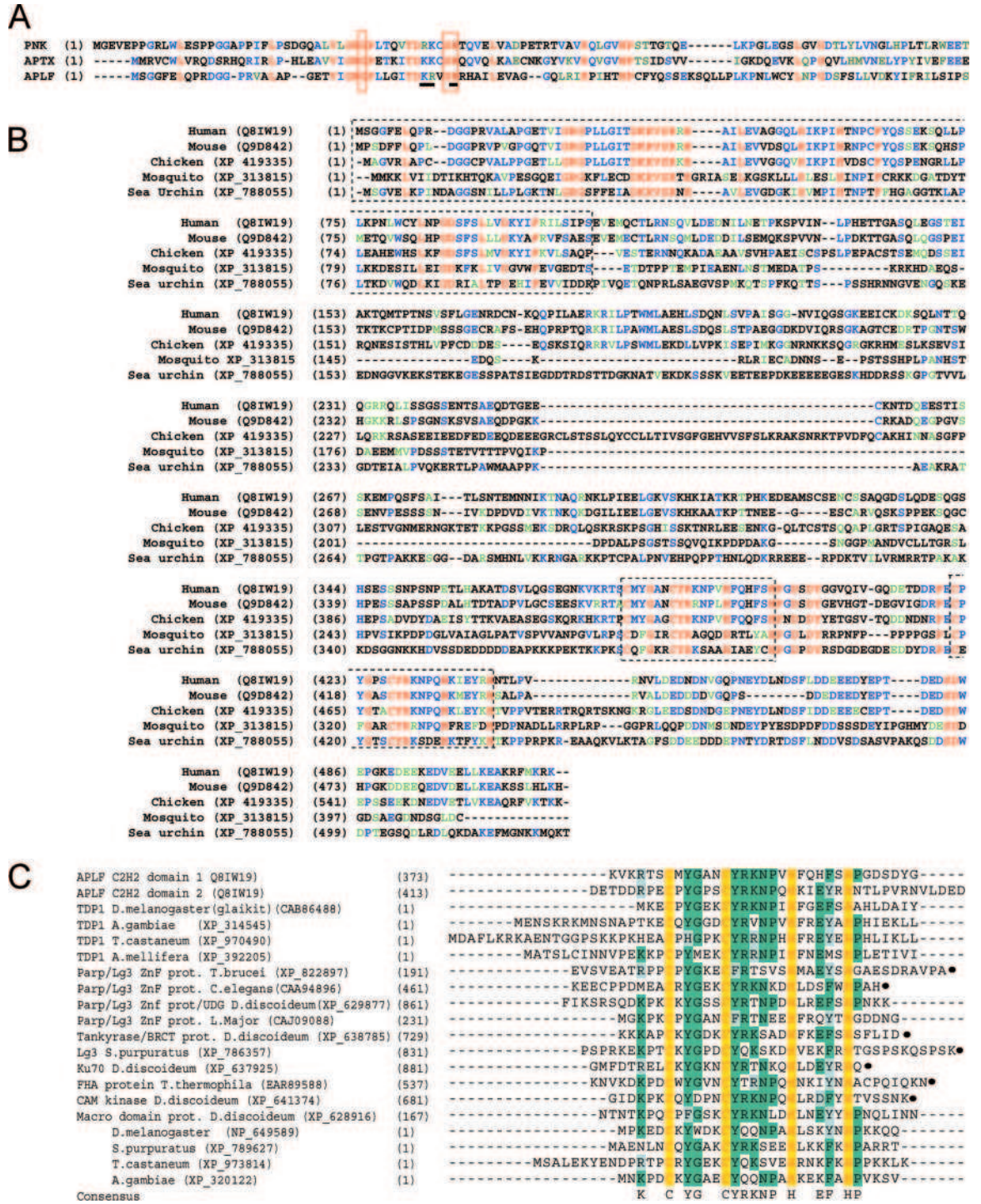

FIG. 1. Conserved FHA and tandem ZnF domains in APLF. (A) Alignment of the FHA domains of APLF, aprataxin (APTX), and PNK. Identical residues are in highlighted in red, highly conserved residues in blue, and similar residues in green. Putative phosphate-binding residues are boxed in red, and the basic residues that are believed to confer specificity for binding CK2-phosphorylated motifs are underlined. (B) APLF protein homologues. BLAST analyses identify multiple homologues of APLF in mouse (*Mus musculus*), chicken (*Gallus gallus*), mosquito (*Anopheles gambiae*), and purple sea urchin (*Strongylocentrotus purpuratus*). Identical residues are in red, highly conserved residues in blue, and blocks of similar residues in green. Dotted boxes denote the amino-terminal FHA domain and the putative tandem ZnFs at the C terminus. (C) BLAST analyses with the C-terminal putative tandem ZnF motif of APLF identifies 18 additional polypeptides that possess this motif in single copy, many of which are likely DNA repair- and DNA damage-associated proteins. Identical residues are boxed in yellow (note that these are the putative metal coordinating residues), highly conserved residues boxed in green, and blocks of similar residues boxed in blue. Black circles denote the C terminus of the polypeptide.

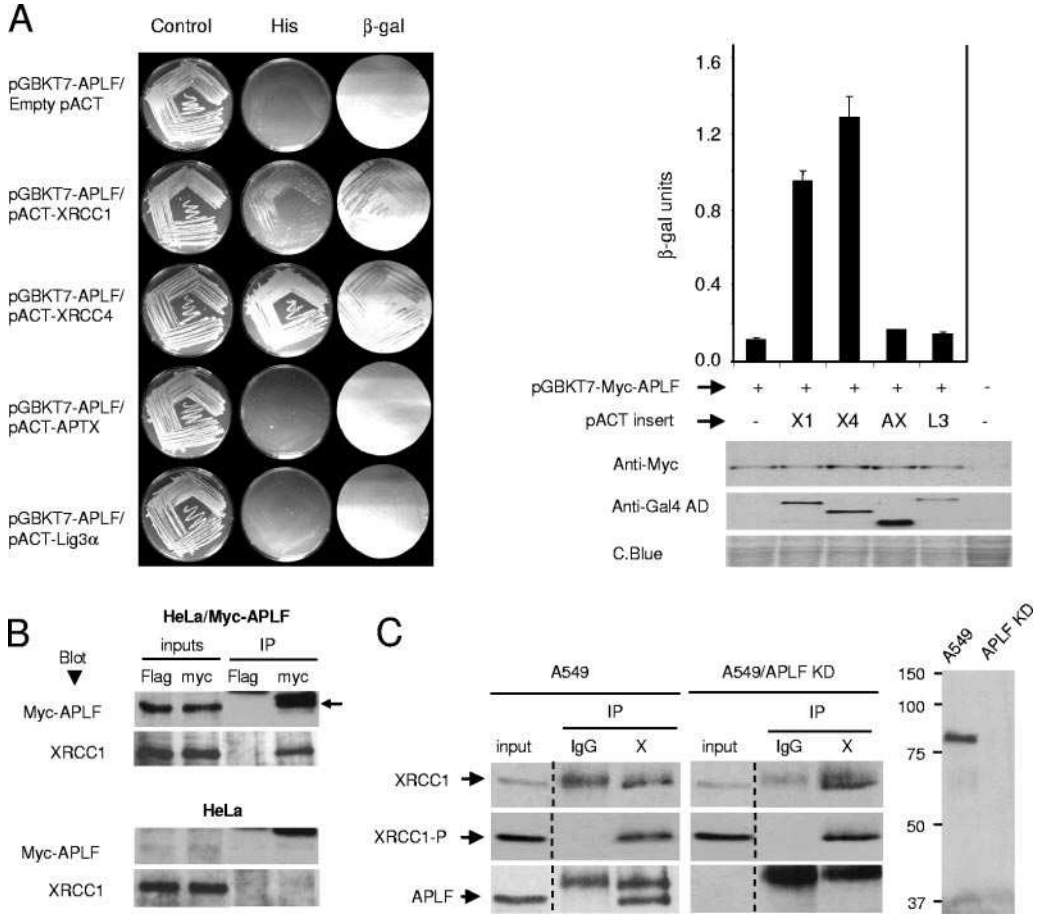

FIG. 2. Interaction of APLF with the DNA strand break repair proteins XRCC1 and XRCC4. (A) (Left) Yeast Y190 cells harboring pGBKT7-*APLF* and the indicated pACT construct were plated onto selective media either containing histidine (Control) or lacking histidine and containing 3-aminotriazole (His) to test for activation of the *His3* reporter gene. The activation of the β-Gal reporter gene was detected using filter lifts from control plates containing histidine. (Right) Results of quantitative β-Gal assays conducted on the Y190 cells described above. Data are the means (±1 standard deviation) for three independent experiments. Expression levels of Myc-APLF (Gal4 binding domain fusion protein) and the activation domain (AD) fusion proteins XRCC1 (X1), XRCC4 (X4), aprataxin (AX), and Lig3α (L3) in the yeast cultures employed for the quantitative assays were determined by immunoblotting with anti-Myc or anti-Gal4 AD antibodies. Yeast cell extract from untransformed Y190 cells was included as an immunoblotting negative control (far right lane). Protein loading was assessed with Coomassie blue (C.Blue). (B) Levels of XRCC1 and Myc-APLF proteins present in total cell extracts (inputs) and in anti-FLAG or anti-Myc immunoprecipitates (IP) from Myc-APLF transiently transfected (HeLa/Myc-APLF) (top) or mock-transfected (HeLa) (bottom) HeLa cells. The position of Myc-APLF is indicated by an arrow. The band visible above Myc-APLF is a contaminating antibody band. (C) (Left and middle) Levels of endogenous XRCC1 and APLF present in total cell extracts (input) and in mouse IgG or anti-XRCC1 immunoprecipitates (IP) from A549 cells stably harboring empty pSuper (A549) or the pSuper-APLF RNAi construct (A549/APLF KD). Note that XRCC1 was detected using both standard anti-XRCC1 (SK3188) polyclonal antibody (top) and anti-phosphorylated XRCC1 (pS485/pT488) antibody (BL610; Bethyl Laboratories) (middle). APLF was detected using the rabbit anti-APLF polyclonal antibody SK3595 (bottom). (Right) Immunoblot of total cell extracts from the A549 and A549/APLF KD cell lines described above with SK3595 to demonstrate the specificity of this anti-APLF antibody.

panels), neither protein bound to control slots blotted with CK2 reaction products lacking XRCC1-His (Fig. 3C, bottom left panel). In contrast to His-APLF and His-APLF$^{1-166}$, a C-terminal fragment of His-APLF (His-APLF$^{360-511}$) containing the putative C_2H_2 ZnFs failed to interact with CK2-phosphorylated XRCC1-His (Fig. 3C, right panel). Similar results were observed by far-Western blotting, in which the CK2-phosphorylated XRCC1-His protein probe detected His-APLF and His-APLF$^{1-166}$, but not His-APLF$^{360-511}$, proteins present on renatured Western blots (Fig. 3D). We conclude from these experiments that the FHA domain in APLF interacts with CK2-phosphorylated XRCC1.

To further examine whether APLF is a component of the DNA damage response, we compared the subcellular localization patterns of endogenous XRCC1 and APLF in human A549 cells following UVA laser irradiation. As expected, XRCC1 rapidly accumulated (within 3 min) at sites of UVA damage (Fig. 4A). More significantly, APLF colocalized and accumulated with XRCC1 at these sites, confirming that APLF is a component of the response to UVA-induced cellular damage. To examine the relationship between XRCC1 and APLF in more detail, we compared the subcellular localization patterns of YFP- and RFP-tagged human APLF and XRCC1 before and after treatment with H_2O_2 in transiently transfected *XRCC1* mutant CHO cells (EM9 cells). Whereas RFP-XRCC1 was largely or entirely nuclear in all transfected EM9 cells,

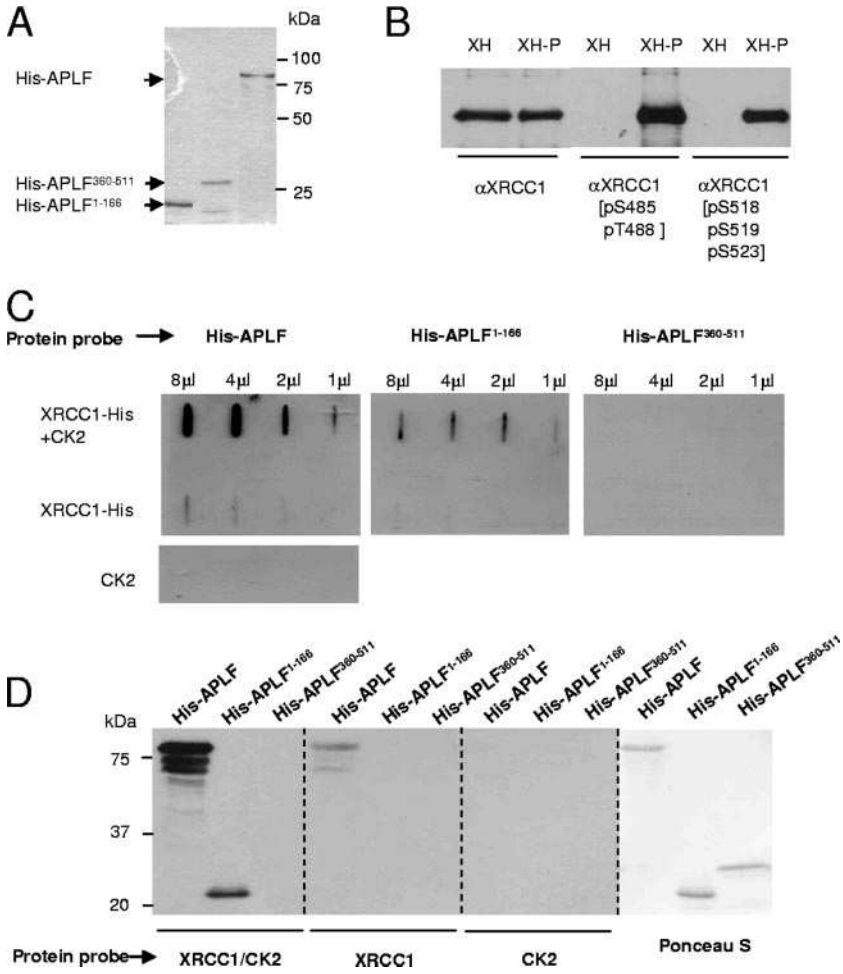

FIG. 3. APLF preferentially interacts with CK2-phosphorylated XRCC1 in vitro. (A) One microgram of recombinant human His-APLF, His-APLF$^{1-166}$, or His-APLF$^{360-511}$ was fractionated by SDS-PAGE and stained with Coomassie blue. (B) Aliquots of mock-phosphorylated (XH) or CK2-phosphorylated (XH-P) recombinant human XRCC1-His were fractionated by SDS-PAGE and immunoblotted with anti-XRCC1 polyclonal antibody (SK3188) (αXRCC1), anti-phosphoserine 485/phosphothreonine 488 XRCC1 polyclonal antibody (BL610; Bethyl Labs) (pS485/pT488), or BL603 anti-phosphoserine 518/phosphothreonine 519/phosphothreonine 523 XRCC1 polyclonal antibody (BL603; Bethyl Labs) (pS518/pT519/pT523). (C) Nitrocellulose membranes slot blotted with 1- to 8-μl aliquots of phosphorylation reaction mixtures containing XRCC1-His alone (0.125 to 1 μg of XRCC1, respectively), CK2 alone, or both XRCC1-His (0.125 to 1 μg) and CK2 (XRCC1-His+CK2) were incubated with His-APLF, His-APLF$^{1-166}$, or His-APLF$^{360-511}$ protein probes, as indicated. Filter-bound APLF was then detected using anti-APLF polyclonal antibody, which recognizes all three recombinant APLF proteins (data not shown). (D) Three micrograms of His-APLF, His-APLF$^{1-166}$, or His-APLF$^{360-511}$ was fractionated by SDS-PAGE in quadruplicate, transferred to nitrocellulose, renatured, and incubated with protein probes comprised of mock phosphorylation reaction mixtures containing XRCC1-His protein alone (XRCC1), CK2 phosphorylation reaction mixtures containing XRCC1-His and CK2 (XRCC1/CK2), or CK2 phosphorylation reaction mixtures lacking XRCC1-His (CK2). The fourth replicate was stained with Ponceau S. Filter-bound XRCC1-His was subsequently detected using anti-XRCC1 antibody.

YFP-APLF was largely nuclear or pancellular in ~60% of cells in the presence of RFP-XRCC1 and largely cytosolic or pancellular in ~90% of cells in the absence of RFP-XRCC1 (Fig. 4B and C, left panel). The fraction of cells with largely nuclear YFP-APLF transiently increased after H_2O_2 treatment in an RFP-XRCC1-dependent manner (Fig. 4C, middle and right panels). The presence of a large proportion of cells with largely nuclear YFP-APLF was also dependent on a functional FHA domain, because the YFP-APLF^{R27A} protein harboring a mutated FHA domain was largely cytoplasmic or pancellular in most cells both before and after H_2O_2 treatment, even in the presence of RFP-XRCC1 (Fig. 4C). We conclude that RFP-XRCC1 promoted the nuclear import or retention of YFP-APLF in these experiments in a manner that was stimulated by oxidative DNA damage and which required the APLF FHA domain.

In the majority (~83%) of cotransfected cells, YFP-APLF and RFP-XRCC1 colocalized in subnuclear foci after H_2O_2 treatment (Fig. 4D and 5A, left panel). In contrast, far fewer focus-positive cells (~15%) were observed in EM9 cells transfected with either YFP-APLF alone or a combination of YFP-APLF^{R27A} and RFP-XRCC1 (Fig. 5A). These data suggest that RFP-XRCC1 stimulates the accumulation of YFP-APLF at oxidative DNA strand breaks but that it is not essential for this process. To examine whether this effect of RFP-XRCC1 reflected its impact on the nuclear localization of YFP-APLF, we created YFP-nls-APLF^{R27A}, a derivative of YFP-APLF^{R27A} in which we engineered an SV40 nuclear localization signal

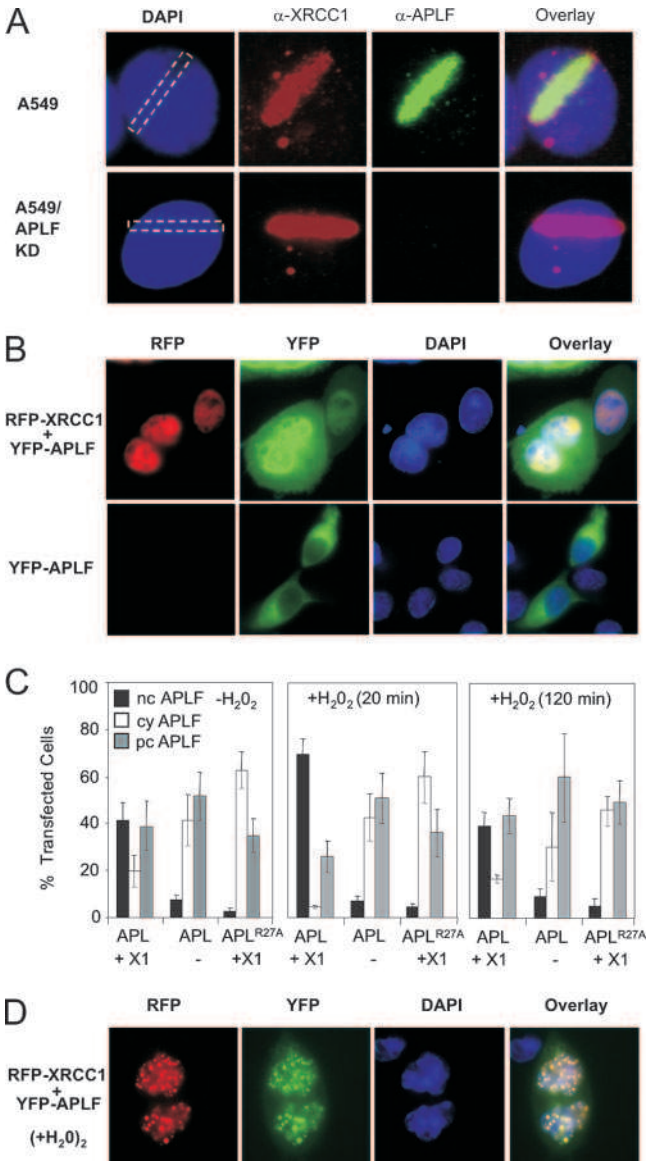

FIG. 4. XRCC1 promotes DNA damage-associated subcellular redistribution of APLF. (A) Indirect immunofluorescence analysis of endogenous XRCC1 and APLF accumulation at sites of UVA irradiation. Human A549 cells were preincubated with Hoechst 33258 (10 μg/ml) for 10 min and irradiated within the area indicated (left panel, dotted white box) with a UVA laser (351 nm). Three minutes after exposure, cells were fixed and labeled with mouse anti-XRCC1 MAb and rabbit anti-APLF SK3595 polyclonal antibody, followed by goat Alexa Fluor 555-conjugated anti-mouse (red) and goat Alexa Fluor 488-conjugated anti-rabbit (green) secondary antibodies. DNA was counterstained with DAPI (blue). (B) Subcellular localization of YFP-APLF protein transiently expressed alone or in combination with RFP-XRCC1 in *XRCC1* mutant EM9 CHO cells. Note that the images included here depict cells with largely nuclear (top) or largely cytoplasmic (bottom) YFP-APLF. (C) Quantitation of the fraction of transiently transfected HeLa cells expressing YFP-APLF or YFP-APLF^{R27A} alone (−) or in combination with RFP-XRCC1 (+X1) in which the recombinant APLF is largely nuclear (nc), largely cytoplasmic (cy), or pancellular (pc). Prior to analysis, cells were either untreated or treated, as indicated, with 10 mM H_2O_2 for 10 min, followed by 20 min or 2 h in drug-free medium to allow recovery. (D) Subcellular localization of YFP-APLF protein transiently expressed alone or in combination with RFP-XRCC1 in H_2O_2-treated *XRCC1* mutant EM9 CHO cells.

(NLS). As expected, YFP-nls-APLF^{R27A} was largely or entirely nuclear and, moreover, accumulated extensively at oxidative DNA strand breaks (Fig. 5A, right panel). These data suggest that XRCC1 facilitates the accumulation of APLF at oxidative SSBs by promoting the nuclear import of APLF, in part at least.

In contrast to RFP-XRCC1, RFP-XRCC4 did not form measurable subnuclear foci after H_2O_2 and had little or no effect on the subcellular localization of YFP-APLF when expressed in *XRCC4* mutant XR-1 CHO cells (data not shown). However, we did note that large numbers (~40%) of XR-1 cells possessed YFP-APLF or YFP-APLF^{R27A} foci after H_2O_2 treatment (data not shown). This most likely reflects the XRCC1-independent recruitment/accumulation of recombinant APLF at DNA strand breaks that was observed, albeit to a lesser extent, in EM9 cells. We considered the possibility that the XRCC1-independent recruitment/accumulation of APLF at sites of oxidative DNA damage might be mediated via the putative C_2H_2 ZnF motifs. To examine this possibility, we expressed derivatives of APLF in which the two putative zinc coordinating cysteine residues in the first (YFP-APLF^{zfm1}) or second (YFP-APLF^{zfm2}) ZnF were mutated to alanine. Neither of the ZnF mutations reduced XRCC1-dependent nuclear import/retention of YFP-APLF in untreated EM9 cells, although the ZFM1 mutation did reduce the XRCC1-dependent increase in nuclear YFP-APLF observed after H_2O_2 treatment (Fig. 5B, right panel). The ZFM1 mutation also reduced the formation of YFP-APLF nuclear foci in the presence of XRCC1, by ~30% (Fig. 5C, left panel). More significantly, however, the XRCC1-independent accumulation of YFP-APLF in nuclear foci was reduced by the ZFM2 mutation and ablated by the ZNF1 mutation (Fig. 5C, right panel). These data confirm that the tandem ZnF motif is required for XRCC1-independent recruitment/accumulation of APLF at sites of oxidative DNA strand breakage.

To examine whether the tandem ZnF promoted XRCC1-independent accumulation of YFP-APLF at sites of oxidative DNA damage through an impact on nuclear localization, we employed derivatives of YFP-APLF and YFP-APLF^{ZnF1} that harbored an SV40 NLS, denoted YFP-nls-APLF and YFP-nls-APLF^{ZnF1}, respectively. While both YFP-nls-APLF and YFP-nls-APLF^{ZnF1} were able to assemble into subnuclear foci in the presence of XRCC1, only YFP-nls-APLF did so in the absence of RFP-XRCC1 (Fig. 5D, left and middle panels). Thus, the addition of an NLS did not circumvent the requirement for the tandem ZnF, suggesting that the ZnF fulfills a function other than increasing the nuclear import/retention of YFP-APLF. Interestingly, we noted in these experiments that RFP-XRCC1 stimulated the assembly of YFP-nls-APLF nuclear foci, despite the presence of an NLS, and did so in a manner that was dependent on an intact FHA domain (Fig. 5D, middle and right panels). This suggests that the impact of the XRCC1-APLF interaction extends beyond its ability to promote APLF nuclear import/retention. In summary, we conclude from these experiments that the accumulation of YFP-APLF at oxidative DNA strand breaks is promoted by at least three mechanisms: two that are dependent on FHA domain-mediated interaction with XRCC1, including one that involves increased nuclear import/retention of APLF, and one that is

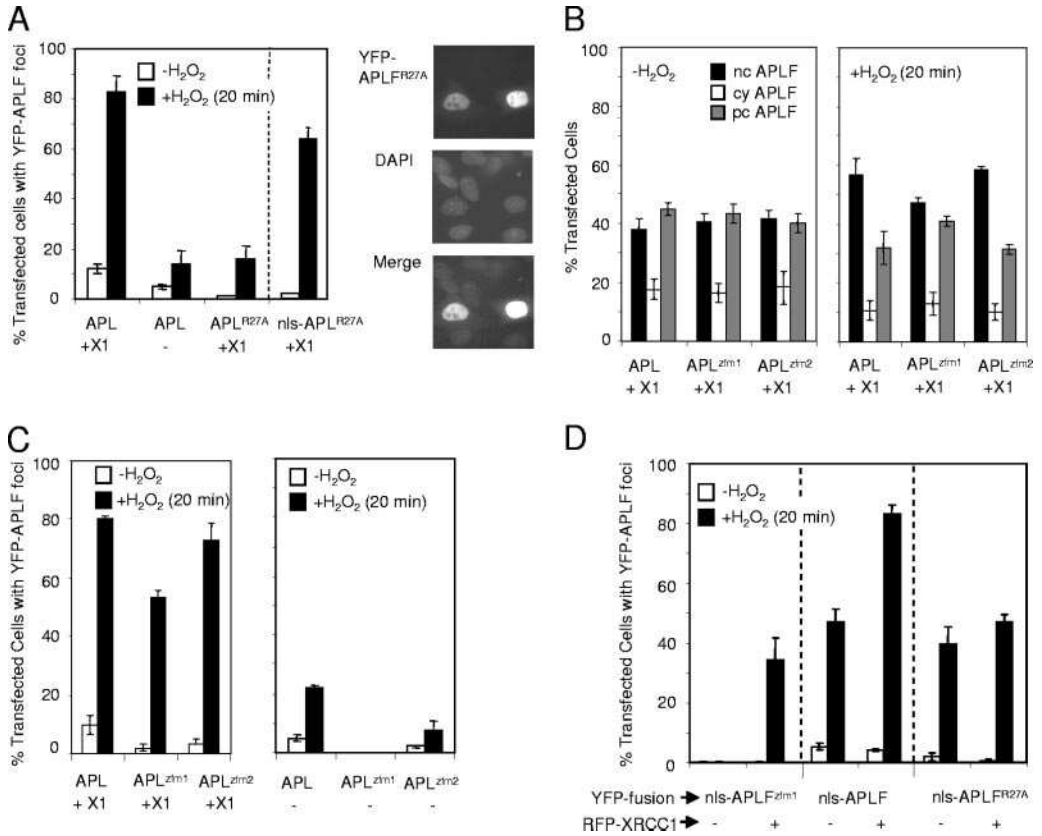

FIG. 5. A novel tandem ZnF motif in APLF mediates XRCC1-independent recruitment/accumulation at sites of oxidative DNA damage. (A) Quantification of the fraction of untreated (open bars) and H_2O_2-treated (filled bars) *XRCC1* mutant EM9 CHO cells containing YFP-APLF (APL), YFP-APLF^{R27A} (APL^{R27A}), or YFP-nls-APLF^{R27A} (nls-APL^{R27A}) nuclear foci in the presence (+X1) or absence (−) of cotransfected mRFP-XRCC1. All data are the means (±1 standard error) for three or more independent experiments. Confirmation of the complete nuclear localization of YFP-nls-APLF^{R27A} is shown on the right. (B) Quantitation of the fraction of transiently transfected HeLa cells coexpressing RFP-XRCC1 and YFP-APLF (APL+X1), YFP-APLF^{zfm1} (APL^{zfm1}+X1), or YFP-APLF^{zfm2} (APL^{zfm2}+X2) in which the recombinant APLF is largely nuclear (nc), largely cytoplasmic (cy), or pancellular (pc). Prior to analysis, cells were either untreated or treated, as indicated, with 10 mM H_2O_2 for 10 min, followed by 20 min in drug-free medium to allow repair. (C) Quantitation of the fraction of transiently transfected HeLa cells with YFP-APLF (APL), YFP-APLF^{zfm1} (APL^{zfm1}), or YFP-APLF^{zfm2} (APL^{zfm2}) subnuclear foci in the presence (left) or absence (right) of cotransfected RFP-XRCC1 (X1). Prior to analysis, cells were either untreated or treated, as indicated, with 10 mM H_2O_2 for 10 min, followed by 20 min or 2 h in drug-free medium to allow recovery. (D) Quantitation of the fraction of transiently transfected HeLa cells with YFP-nls-APLF (nls-APLF), YFP-nls-APLF^{zfm1} (nls-APLF^{zfm1}), or YFP-nls-APLF^{R27A} (nls-APLF^{R27A}) subnuclear foci in the presence (+) or absence (−) of cotransfected RFP-XRCC1. Prior to analysis, cells were either untreated or treated, as indicated, with 10 mM H_2O_2 for 10 min, followed by 20 min or 2 h in drug-free medium to allow recovery.

independent of XRCC1 but dependent on the tandem ZnF motif.

To further examine the involvement of APLF in the response to DNA damage, we compared its electrophoretic mobilities before and after treatment with gamma rays or H_2O_2. Notably, the mobility of endogenous APLF during SDS-PAGE decreased after treatment with either H_2O_2 or ionizing radiation (IR) in wild-type cells and in aprataxin-defective AOA1 primary fibroblasts (Fig. 6A). However, this shift in electrophoretic mobility was not detected in ataxia telangiectasia fibroblasts lacking the DSB-responsive protein kinase ATM. These data support the idea that APLF is involved in the cellular response to DSBs. To examine whether APLF is required for chromosomal DNA single- and double-strand break repair, we mock depleted or depleted APLF or XRCC1 from differentiated/noncycling SH-SY5Y neuroblastoma cells by transient siRNA transfection (Fig. 6B, left panel). Whereas the type of siRNA did not affect the level of DNA strand breaks induced by IR, as measured by alkaline comet assays, the rate at which DNA strand breaks declined was significantly delayed in both XRCC1- and APLF-depleted cells (Fig. 6C). It is likely that the delay observed here reflects a defect in SSBR, because >95% of the total breaks induced by IR are SSBs (4). To examine the rate of DSBR, we quantified the level of γ-H2AX, an established marker of DSBs (26, 27), in gamma ray-treated SH-SY5Y neuroblastoma cells that were depleted of APLF as described above or in A549 cells that were stably depleted of APLF (Fig. 5B, right panels). We consistently observed in these experiments that γ-H2AX foci declined at significantly reduced rates in both APLF-depleted neuroblastoma cells and A549 cells following 1 to 3 Gy of IR (Fig. 6D). In contrast, repair rates were normal in XRCC1-depleted SH-SY5Y cells, consistent with the absence of a measurable DSBR defect in these cells (Fig. 6D, right panel).

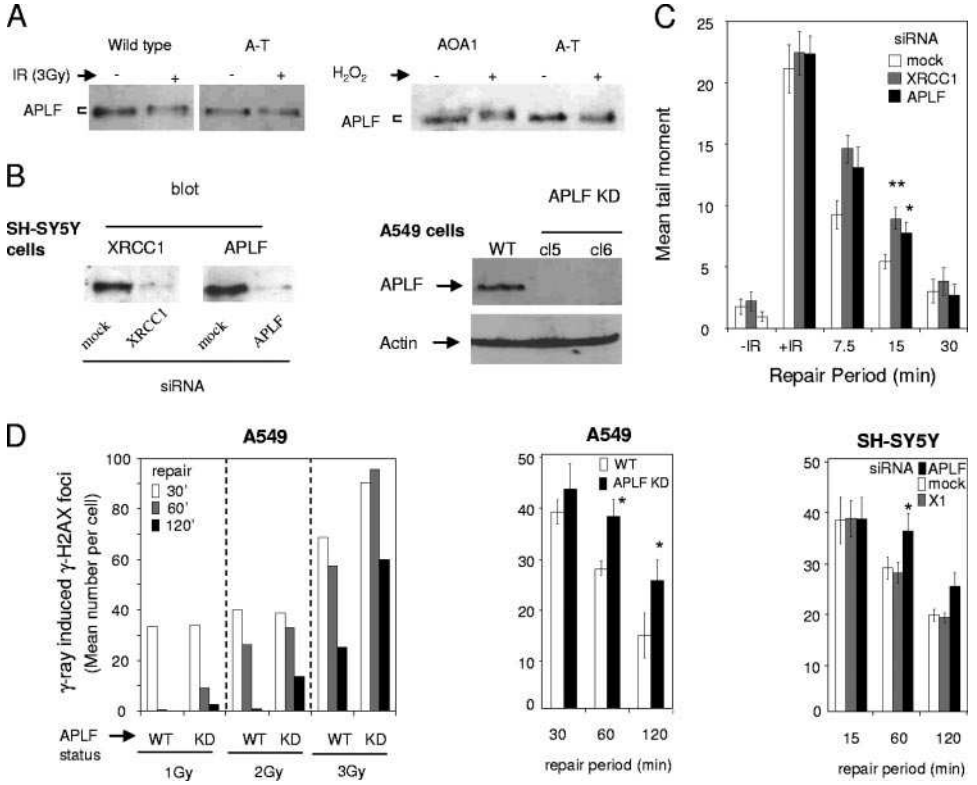

FIG. 6. Delayed rates of DNA strand break repair in APLF-depleted human cells. (A) Comparison of the electrophoretic mobilities of endogenous APLF in normal, ataxia telangiectasia (A-T), and AOA1 primary human fibroblasts before and after treatment with either gamma rays (3 Gy) (left) or 10 mM H_2O_2 for 10 min (right), followed by recovery in drug-free medium for 20 to 30 min. APLF was detected by immunoblotting with anti-APLF SK3595 polyclonal antibody. (B) Cell extracts from quiescent SH-SY5Y neuroblastoma cells mock transfected or transiently transfected with XRCC1 or APLF siRNA (left) or from cycling A549 cells stably transfected with empty pSuper vector (WT) or the pSuper APLF knockdown construct (clones 5 and 6 [cl5 and cl6]) (right) were immunoblotted for levels of XRCC1, APLF, and actin as indicated. (C) Quantitation of DNA strand breakage, as measured by alkaline comet assays, in untreated quiescent SH-SY5Y neuroblastoma cells or in irradiated (20 Gy of gamma rays) cells following a subsequent incubation for the indicated periods to allow time for repair. Cells were mock transfected or transiently transfected with XRCC1 or APLF siRNA prior to irradiation. In each experiment, the average tail moment for 100 cells per sample was calculated and the plotted data are the means (±1 standard error) for four independent experiments. (D) (Left and middle) Quantitation of DNA double-strand breakage, as measured by γ-H2AX assays, in cycling A549 cells stably transfected with empty pSuper vector (WT) or pSuper APLF knockdown construct (KD) (cl5) after 1 to 3 Gy (left) or 2 Gy (middle) of gamma rays, followed by incubation for the indicated periods (30 to 120 min) to allow time for DNA repair. The mean number of gamma ray-induced γ-H2AX foci per cell is plotted, and the data are from a single experiment in the left panel and are the means for three independent experiments in the middle panel. (Right) Quantitation of DNA double-strand breakage, as measured by γ-H2AX assays, in quiescent SH-SY5Y cells after γ-irradiation (2 Gy), followed by a subsequent repair/incubation for 15 to 120 min. Cells were either mock transfected or transiently transfected with XRCC1 or APLF siRNA prior to irradiation. The mean number of γ-H2AX foci per cell is plotted, and the data are the means for three independent experiments. Note that in the γ-H2AX experiments, less than one focus per cell was visible prior to, or immediately after, irradiation. Asterisks denote statistical significance (paired *t* test) with wild-type or mock-depleted cells. *, $P < 0.05$; **, $P < 0.01$.

DISCUSSION

We describe here a new component of the DNA single- and double-strand break repair machinery. This protein is a previously uncharacterized ORF (C2orf13) that we have denoted APLF based on the presence of an aprataxin- and PNK-like FHA domain at its amino terminus. Consistent with the presence of this domain, APLF interacts with both XRCC1 and XRCC4, the same components of the single- and double-strand break repair machinery that are bound by PNK and aprataxin (11, 12, 14, 16, 22, 33). Moreover, similar to the situation with PNK and aprataxin, the interaction of XRCC1 with full-length APLF in vitro or with a fragment of APLF containing the FHA domain was largely dependent on the phosphorylation of XRCC1 by CK2. Intriguingly, a yeast two-hybrid screen employing APLF as bait recovered not only multiple clones of both XRCC1 and XRCC4 but also multiple clones of XRCC5 (Ku86). Of 109 cDNA clones recovered, 6 encoded XRCC1, 15 encoded XRCC4, and 7 encoded XRCC5 (Ku86) (data not shown). APLF may thus associate with the nonhomologous end-joining machinery through interactions with both XRCC4 and the Ku86 heterodimer.

Direct evidence of a role for APLF in the cellular response to DNA damage emerged from the observations that endogenous APLF accumulates at sites of UVA laser damage in human A549 cells and that recombinant YFP-APLF accumulates in subnuclear foci in H_2O_2-treated CHO cells. Whereas the UVA laser tracts most likely contain sites with both single- and double-strand breaks (data not shown), the H_2O_2-induced foci most likely reflect just SSBs. This is because they colocalize and are stimulated by RFP-XRCC1 and because they do

not significantly colocalize with sites of γ-H2AX (data not shown). In addition, we failed to detect accumulation of the DSBR protein XRCC4 in H_2O_2-induced subnuclear foci under the same experimental conditions. It is also noteworthy that, in collaborative experiments with Akira Yasui, we observed the accumulation of YFP-APLF at UVA laser-induced damage under conditions where SSBs are selectively induced (19; unpublished observations).

The ability of RFP-XRCC1 to stimulate the accumulation of YFP-APLF in subnuclear foci most likely reflected, at least in part, the impact of recombinant XRCC1 on the nuclear import or retention of YFP-APLF. This is because the addition of an NLS to YFP-APLF circumvented the requirement of RFP-XRCC1 for high levels of YFP-APLF nuclear foci. However, these experiments do not rule out an additional role(s) for XRCC1 during the accumulation of YFP-APLF at sites of DNA damage. This is because the NLS had a much greater impact on the nuclear import/retention of YFP-APLF than did recombinant RFP-XRCC1, perhaps thereby masking additional roles for XRCC1. Indeed, consistent with this notion, the coexpression of RFP-XRCC1 stimulated the appearance of YFP-nls-APLF nuclear foci, albeit to a lesser extent than YFP-APLF foci (fivefold versus twofold), despite the presence of an NLS. The nature of the alternative mechanism by which XRCC1 might promote the accumulation of YFP-APLF at sites of oxidative DNA damage is not known. However, since this mechanism required an intact FHA domain in APLF, one attractive possibility is that it reflects the scaffolding role of XRCC1. A similar explanation has been suggested for the observation that XRCC1 also promotes the accumulation of aprataxin, PNK, and DNA polymerase β at sites of H_2O_2-induced DNA damage (21; unpublished observations).

H_2O_2-induced YFP-APLF foci were observed in 15 to 40% of CHO cells in the absence of XRCC1, and a similar fraction of YFP-APLF focus-positive cells was observed when RFP-XRCC1 was coexpressed with YFP-APLF lacking an intact FHA domain. Thus, although greatly stimulated by the coexpression of recombinant XRCC1, the recruitment/accumulation of YFP-APLF at sites of oxidative DNA damage can occur independent of XRCC1. Intriguingly, this XRCC1-independent mode of APLF recruitment/accumulation required the two tandem ZnF motifs, supporting the notion that these structures represent a novel class of DNA strand break-responsive motifs. The amino acid sequences of the tandem ZnFs in APLF appear to be distinct from those present in other SSBR/DSBR proteins, such as aprataxin and poly(ADP-ribose) polymerase 1, as indicated by the limited number of proteins detected as containing this motif in database searches (Fig. 1C). It is not yet clear what function these putative ZnFs fulfill, but the presence of this structure in a variety of other DNA repair and DNA metabolic proteins suggests that it is an important one. The impact of the ZnFs on the XRCC1-independent recruitment/accumulation of YFP-APLF at sites of oxidative DNA damage was not mediated via increased nuclear import or retention of APLF, because the addition of an NLS did not compensate for the absence of intact ZnFs. We suggest that the ZnF may bind to DNA strand breaks directly, thereby promoting XRCC1-independent recruitment of APLF at sites of chromosomal damage.

In contrast to RFP-XRCC1, RFP-XRCC4 did not promote the redistribution of APLF to nuclei or the accumulation of APLF in H_2O_2-induced subnuclear foci. This may reflect the nature of the cellular response to DSBs because accumulation in discrete subnuclear foci does not appear to be a general feature of nonhomologous end-joining enzymes such as XRCC4 and Ku following oxidative stress. However, further evidence that APLF is involved in the response to DSBs was suggested by the change in the electrophoretic mobility of this protein induced by IR or H_2O_2. Significantly, this phenomenon was dependent on the DSB sensor protein kinase ATM, suggesting that APLF is phosphorylated in an ATM-dependent manner in response to DSBs, though we cannot rule out that ATM is activated in this context by some other type of lesion or event. It also remains to be determined whether APLF is a substrate for ATM or whether APLF is modified via ATM indirectly.

Alkaline comet and γ-H2AX assays suggested that the depletion of APLF by siRNA retards the rate of DNA single- and double-strand break repair at early times after IR. We observed a DSBR defect in both proliferating A549 lung carcinoma cells and noncycling SH-SY5Y neuroblastoma cells, as measured by γ-H2AX staining. However, using alkaline comet assays, we detected a DNA strand break repair defect only in noncycling SH-SY5Y cells (data not shown). Since alkaline comet assays measured primarily SSBs in these experiments, due to the abundance of SSBs relative to DSBs induced by IR (~20:1), we suggest that this reflects a difference in the redundancies of APLF during SSBR in proliferating versus noncycling cells. Differences in polypeptide requirements during SSBR in S-phase versus nonreplicating cells have been reported previously (24, 29). The impact of APLF depletion on DNA strand break repair rates was subtle, though in the case of SSBR, it was no less subtle than in cells depleted of XRCC1, which is the archetypal SSBR protein (7, 32). The relatively small impact on repair rates observed in these experiments could thus be due to the incomplete depletion of XRCC1 and APLF by siRNA. Alternatively, it is possible that APLF is required for the rapid repair of only a subset of DNA strand breaks, such as those with specific types of DNA termini. This is also most likely the case for aprataxin, which removes rare 5′ AMP adducts from DNA strand breaks in vitro but does not have a measurable impact on global rates of DNA strand break repair in vivo (1).

What role might APLF play during DNA strand break repair? Given that APLF most likely binds the same regions of XRCC1 and XRCC4 that are bound by PNK and aprataxin, both of which are end processing enzymes, it is tempting to speculate that APLF fulfills or facilitates a similar activity. This suggests a model in which CK2-phosphorylated XRCC1 or XRCC4 can recruit one of at least three different end processing activities to an SSB or DSB, depending on the nature of the damaged termini. The unusual nature of the tandem ZnFs may be informative in this respect. Combined sequence/structure database analyses assign this motif as a tandem ZnF most closely related to the CCCH tandem ZnFs present in the tristetrapolin family of mRNA binding proteins (3, 17). Interestingly, these tandem ZnFs appear to be required to facilitate the deadenylation of 3′ poly(A) tails of specific mRNAs, most likely through the recruitment of an RNase (18). Although they share some similarities, the APLF tandem ZnFs and

tristetraprolin family ZnFs are clearly distinct, most notably in the spacing between the zinc coordinating residues and the absence of specific residues critical for mRNA binding. It is thus tempting to speculate that the tandem putative ZnFs in APLF target DNA rather than RNA, thereby facilitating the processing of a specific type of DNA 3′ terminus.

ACKNOWLEDGMENTS

This work was supported by MRC grants G0001259, G0400959, and G0600776 and an MRC studentship to N.I.

We thank Roger Phillips in the Sussex Centre for Advanced Microscopy for help with the UVA laser experiments.

REFERENCES

1. **Ahel, I., U. Rass, S. F. El-Khamisy, S. Katyal, P. M. Clements, P. J. McKinnon, K. W. Caldecott, and S. C. West.** 2006. The neurodegenerative disease protein aprataxin resolves abortive DNA ligation intermediates. Nature **443:**713–716.
2. **Bernstein, N. K., R. S. Williams, M. L. Rakovszky, D. Cui, R. Green, F. Karimi-Busheri, R. S. Mani, S. Galicia, C. A. Koch, C. E. Cass, D. Durocher, M. Weinfeld, and J. N. Glover.** 2005. The molecular architecture of the mammalian DNA repair enzyme, polynucleotide kinase. Mol. Cell **17:**657–670.
3. **Blackshear, P. J.** 2002. Tristetraprolin and other CCCH tandem zinc-finger proteins in the regulation of mRNA turnover. Biochem. Soc. Trans. **30:**945–952.
4. **Bradley, M. O., and K. W. Kohn.** 1979. X-ray induced DNA double strand break production and repair in mammalian cells as measured by neutral filter elution. Nucleic Acids Res. **7:**793–804.
5. **Breslin, C., P. M. Clements, S. F. El-Khamisy, E. Petermann, N. Iles, and K. W. Caldecott.** 2006. Measurement of chromosomal DNA single-strand breaks and replication fork progression rates. Methods Enzymol. **409:**410–425.
6. **Caldecott, K. W.** 2003. DNA single-strand break repair and spinocerebellar ataxia. Cell **112:**7–10.
7. **Caldecott, K. W.** 2003. XRCC1 and DNA strand break repair. DNA Repair (Amsterdam) **2:**955–969.
8. **Caldecott, K. W., J. D. Tucker, L. H. Stanker, and L. H. Thompson.** 1995. Characterization of the XRCC1-DNA ligase III complex in vitro and its absence from mutant hamster cells. Nucleic Acids Res. **23:**4836–4843.
9. **Campbell, R. E., O. Tour, A. E. Palmer, P. A. Steinbach, G. S. Baird, D. A. Zacharias, and R. Y. Tsien.** 2002. A monomeric red fluorescent protein. Proc. Natl. Acad. Sci. USA **99:**7877–7882.
10. **Chappell, C., L. A. Hanakahi, F. Karimi-Busheri, M. Weinfeld, and S. C. West.** 2002. Involvement of human polynucleotide kinase in double-strand break repair by non-homologous end joining. EMBO J. **21:**2827–2832.
11. **Clements, P. M., C. Breslin, E. D. Deeks, P. J. Byrd, L. Ju, P. Bieganowski, C. Brenner, M. C. Moreira, A. M. Taylor, and K. W. Caldecott.** 2004. The ataxia-oculomotor apraxia 1 gene product has a role distinct from ATM and interacts with the DNA strand break repair proteins XRCC1 and XRCC4. DNA Repair (Amsterdam) **3:**1493–1502.
12. **Date, H., S. Igarashi, Y. Sano, T. Takahashi, H. Takano, S. Tsuji, M. Nishizawa, and O. Onodera.** 2004. The FHA domain of aprataxin interacts with the C-terminal region of XRCC1. Biochem. Biophys. Res. Commun. **325:**1279–1285.
13. **Date, H., O. Onodera, H. Tanaka, K. Iwabuchi, K. Uekawa, S. Igarashi, R. Koike, T. Hiroi, T. Yuasa, Y. Awaya, T. Sakai, T. Takahashi, H. Nagatomo, Y. Sekijima, I. Kawachi, Y. Takiyama, M. Nishizawa, N. Fukuhara, K. Saito, S. Sugano, and S. Tsuji.** 2001. Early-onset ataxia with ocular motor apraxia and hypoalbuminemia is caused by mutations in a new HIT superfamily gene. Nat. Genet. **29:**184–188.
14. **Gueven, N., O. J. Becherel, A. W. Kijas, P. Chen, O. Howe, J. H. Rudolph, R. Gatti, H. Date, O. Onodera, G. Taucher-Scholz, and M. F. Lavin.** 2004. Aprataxin, a novel protein that protects against genotoxic stress. Hum. Mol. Genet. **13:**1081–1093.
15. **Kadkhodayan, S., E. P. Salazar, J. E. Lamerdin, and C. A. Weber.** 1996. Construction of a functional cDNA clone of the hamster ERCC2 DNA repair and transcription gene. Somat. Cell Mol. Genet. **22:**453–460.
16. **Koch, C. A., R. Agyei, S. Galicia, P. Metalnikov, P. O'Donnell, A. Starostine, M. Weinfeld, and D. Durocher.** 2004. Xrcc4 physically links DNA end processing by polynucleotide kinase to DNA ligation by DNA ligase IV. EMBO J. **23:**3874–3885.
17. **Lai, W. S., E. Carballo, J. M. Thorn, E. A. Kennington, and P. J. Blackshear.** 2000. Interactions of CCCH zinc finger proteins with mRNA. Binding of tristetraprolin-related zinc finger proteins to AU-rich elements and destabilization of mRNA. J. Biol. Chem. **275:**17827–17837.
18. **Lai, W. S., E. A. Kennington, and P. J. Blackshear.** 2003. Tristetraprolin and its family members can promote the cell-free deadenylation of AU-rich element-containing mRNAs by poly(A) ribonuclease. Mol. Cell. Biol. **23:**3798–3812.
19. **Lan, L., S. Nakajima, Y. Oohata, M. Takao, S. Okano, M. Masutani, S. H. Wilson, and A. Yasui.** 2004. In situ analysis of repair processes for oxidative DNA damage in mammalian cells. Proc. Natl. Acad. Sci. USA **101:**13738–13743.
20. **Li, Z., T. Otevrel, Y. Gao, H. L. Cheng, B. Seed, T. D. Stamato, G. E. Taccioli, and F. W. Alt.** 1995. The XRCC4 gene encodes a novel protein involved in DNA double-strand break repair and V(D)J recombination. Cell **83:**1079–1089.
21. **Loizou, J. I., S. F. El-Khamisy, A. Zlatanou, D. J. Moore, D. W. Chan, J. Qin, S. Sarno, F. Meggio, L. A. Pinna, and K. W. Caldecott.** 2004. The protein kinase CK2 facilitates repair of chromosomal DNA single-strand breaks. Cell **117:**17–28.
22. **Luo, H., D. W. Chan, T. Yang, M. Rodriguez, B. P. Chen, M. Leng, J. J. Mu, D. Chen, Z. Songyang, Y. Wang, and J. Qin.** 2004. A new XRCC1-containing complex and its role in cellular survival of methyl methanesulfonate treatment. Mol. Cell. Biol. **24:**8356–8365.
23. **Masson, N., H. C. Hurst, and K. A. Lee.** 1993. Identification of proteins that interact with CREB during differentiation of F9 embryonal carcinoma cells. Nucleic Acids Res. **21:**1163–1169.
24. **Moore, D. J., R. M. Taylor, P. Clements, and K. W. Caldecott.** 2000. Mutation of a BRCT domain selectively disrupts DNA single-strand break repair in noncycling Chinese hamster ovary cells. Proc. Natl. Acad. Sci. USA **97:**13649–13654.
25. **Moreira, M. C., C. Barbot, N. Tachi, N. Kozuka, E. Uchida, T. Gibson, P. Mendonca, M. Costa, J. Barros, T. Yanagisawa, M. Watanabe, Y. Ikeda, M. Aoki, T. Nagata, P. Coutinho, J. Sequeiros, and M. Koenig.** 2001. The gene mutated in ataxia-ocular apraxia 1 encodes the new HIT/Zn-finger protein aprataxin. Nat. Genet. **29:**189–193.
26. **Rogakou, E. P., C. Boon, C. Redon, and W. M. Bonner.** 1999. Megabase chromatin domains involved in DNA double-strand breaks in vivo. J. Cell Biol. **146:**905–916.
27. **Rogakou, E. P., D. R. Pilch, A. H. Orr, V. S. Ivanova, and W. M. Bonner.** 1998. DNA double-stranded breaks induce histone H2AX phosphorylation on serine 139. J. Biol. Chem. **273:**5858–5868.
28. **Stamato, T. D., R. Weinstein, A. Giaccia, and L. Mackenzie.** 1983. Isolation of cell cycle-dependent gamma ray-sensitive Chinese hamster ovary cell. Somatic Cell Genet. **9:**165–173.
29. **Taylor, R. M., D. J. Moore, J. Whitehouse, P. Johnson, and K. W. Caldecott.** 2000. A cell cycle-specific requirement for the XRCC1 BRCT II domain during mammalian DNA strand break repair. Mol. Cell. Biol. **20:**735–740.
30. **Thompson, L. H., K. W. Brookman, L. E. Dillehay, A. V. Carrano, J. A. Mazrimas, C. L. Mooney, and J. L. Minkler.** 1982. A CHO-cell strain having hypersensitivity to mutagens, a defect in DNA strand-break repair, and an extraordinary baseline frequency of sister-chromatid exchange. Mutat. Res. **95:**427–440.
31. **Thompson, L. H., K. W. Brookman, N. J. Jones, S. A. Allen, and A. V. Carrano.** 1990. Molecular cloning of the human *XRCC1* gene, which corrects defective DNA strand break repair and sister chromatid exchange. Mol. Cell. Biol. **10:**6160–6171.
32. **Thompson, L. H., and M. G. West.** 2000. XRCC1 keeps DNA from getting stranded. Mutat. Res. **459:**1–18.
33. **Whitehouse, C. J., R. M. Taylor, A. Thistlethwaite, H. Zhang, F. Karimi-Busheri, D. D. Lasko, M. Weinfeld, and K. W. Caldecott.** 2001. XRCC1 stimulates human polynucleotide kinase activity at damaged DNA termini and accelerates DNA single-strand break repair. Cell **104:**107–117.
34. **Williams, R. S., N. Bernstein, M. S. Lee, M. L. Rakovszky, D. Cui, R. Green, M. Weinfeld, and J. N. Glover.** 2005. Structural basis for phosphorylation-dependent signaling in the DNA-damage response. Biochem. Cell Biol. **83:**721–727.

MOLECULAR AND CELLULAR BIOLOGY, May 2008, p. 3561 Vol. 28, No. 10
0270-7306/08/$08.00+0 doi:10.1128/MCB.00452-08

AUTHOR'S CORRECTION

APLF (C2orf13) Is a Novel Human Protein Involved in the Cellular Response to Chromosomal DNA Strand Breaks

Natasha Iles, Stuart Rulten, Sherif F. El-Khamisy, and Keith W. Caldecott

Genome Damage and Stability Centre, University of Sussex, Falmer, Brighton, Sussex BN1 9RQ, United Kingdom, and Biochemistry Department, Faculty of Pharmacy, Aim Shams University, P.O. Box 11566, Cairo, Egypt

Volume 27, no. 10, p. 3793–3803, 2007. Page 3799: In the legend to Fig. 4C, "HeLa" should read "EM9 CHO."
Page 3800: In the legends to Fig. 5B, C, and D, "HeLa" should read "EM9 CHO."
Page 3793: The postal code for Sussex should read as shown above.